AIAA JOURNAL
Vol. 45, No. 9, September 2007

Optimum Performance of Electron Beam Driven Magnetohydrodynamic Generators for Scramjet Inlet Control

Sergey O. Macheret,* Mikhail N. Shneider,† and Richard B. Miles‡
Princeton University, Princeton, New Jersey 08544

DOI: 10.2514/1.16955

This paper is devoted to the analysis and optimization of magnetohydrodynamic control of forebody flow compression and shock incidence in scramjet-powered vehicles that would fly at Mach 5–8. The short (about 30 cm long) magnetohydrodynamic region is created by placing a magnetic coil with *B*-field strength of several Tesla inside the forebody and ionizing the cold air flow by high-energy electron beams propagating along the magnetic field lines. The Faraday current flowing in the spanwise direction is presumed to be collected with electrodes that are mounted on sidewalls. The purpose of the magnetohydrodynamic device is to restore a shock-on-lip condition at Mach 8 for a vehicle geometry designed for Mach 5, while operating in self-powered mode (the magnetohydrodynamic generated electricity is enough to power the ionizing beams). Location and spatial dimensions of the magnetohydrodynamic region, beam-generated ionization profiles, magnetic field strength, and the magnet size are varied to maximize performance and reduce the magnet size. Two-dimensional inviscid steady-state flow equations are solved jointly with equations describing electron beam-induced ionization profiles, plasma kinetics, vibrational relaxation, and magnetohydrodynamic effects. The model predicts an interesting phenomenon of electric current reversal due to the nonuniformity of velocity, magnetic field, and conductivity in the magnetohydrodynamic region. Vibrational nonequilibrium effects are found to be substantial. Overall, the modeling shows that a considerable reduction in magnet size is possible with the optimum choice of parameters.

Nomenclature

B	=	magnetic field magnitude
B_z	=	z component of magnetic field
$\boldsymbol{E}$	=	electric field
E_y	=	y component of electric field
H	=	width of MHD region (along y)
h	=	altitude
I	=	total current
I_y	=	total Faraday current
j_y	=	Faraday current density
k	=	load factor
k_H	=	total enthalpy ratio
k_m	=	mass capture ratio
k_p	=	static pressure ratio
k_{p_t}	=	total pressure ratio
k_T	=	static temperature ratio
k_ρ	=	density ratio
L_b	=	e-beam penetration depth
M	=	Mach number
M_{design}	=	design Mach number
P_b	=	power of ionizing electron beams
P_J	=	Joule heating rate
$P_{j\times B}$	=	rate of work by $\boldsymbol{j} \times \boldsymbol{B}$ forces
P_{MHD}	=	MHD extracted power
P_V	=	power deposition into vibrational mode of molecules
p_0	=	static pressure
Q_b	=	e-beam power deposition density
R	=	effective radius of the magnet
R_e	=	external resistor
r	=	total electrical resistance of the nonuniform plasma region
S	=	interaction parameter (Stuart number)
T_0	=	static temperature
U_{el}	=	Faraday voltage [per 1 m in the spanwise (y) direction]
u	=	flow velocity
V	=	voltage
x	=	longitudinal coordinate; marching coordinate
y	=	transversal coordinate
z	=	transversal coordinate
z_b	=	z coordinate of upper boundary of computation domain
Δx_{MHD}	=	MHD channel length
η	=	enthalpy extraction ratio
$\eta_{\text{KE,cool}}$	=	cooled kinetic energy efficiency
ρ	=	flow density
σ	=	electrical conductivity

Presented as Paper 3763 at the 34th AIAA Plasmadynamics and Lasers Conference, Orlando, Florida, 23–26 June 2003; received 3 April 2005; revision received 11 March 2007; accepted for publication 7 May 2007.

*Currently Senior Staff Aeronautical Engineer, Skunk Works, Lockheed Martin Aeronautics Company, Palmdale, CA; sergey.macheret@lmco.com. Associate Fellow AIAA.

†Research Scientist, Department of Mechanical and Aerospace Engineering, D-414 Engineering Quadrangle. Senior Member AIAA.

‡Professor, Department of Mechanical and Aerospace Engineering, D-414 Engineering Quadrangle. Fellow AIAA.

I. Introduction

THE geometry, size, and weight of scramjet-powered hypersonic vehicles are largely dictated by the need to compress the ambient low-density air upstream of the combustor [1]. The optimum geometry corresponds to the well-known shock-on-lip (SOL) condition (Fig. 1): the compression ramp shocks converge on the cowl lip, and the reflected shock impinges on the upper boundary of the inlet [1]. Because shock angles are determined by the flight Mach number, the SOL condition cannot be met at Mach numbers higher or lower than the design Mach number [1]. At Mach numbers higher than the design value, the shocks move inside the inlet, causing multiple reflected shocks, loss of stagnation pressure, possible boundary layer separation, and engine unstart. At Mach numbers lower than the design value, a portion of the air compressed by the

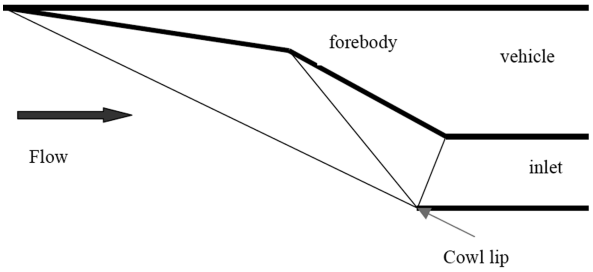

Fig. 1 Design forebody and inlet geometry with shock-on-lip condition.

shock misses the inlet ("spillage"), and the air mass capture decreases.

At off-design Mach numbers, energy addition to or extraction from the flow, using plasmas and various magnetohydrodynamic (MHD) devices, can be considered as an alternative to a variable geometry inlet.

An attractive scenario for MHD inlet control that has been analyzed by several groups [2–11] is to design the vehicle for a relatively low Mach number (for example, Mach 5 or 6), and, at high Mach numbers, move the shocks from inside the inlet back to the cowl lip by an MHD generator device placed at one of the compression ramps (Fig. 3). This method, while providing some flexibility of flow control, would not require any net power to run the MHD device, because the generator mode would be used, and the power requirements for air ionization can be minimized with electron beams as ionizers [2–4,10–17]. Principal disadvantages of the method include stagnation pressure losses due to the inevitable Joule heating, and also weight of the magnet and other hardware.

In our recent paper [3], we demonstrated that this approach to MHD inlet control can yield an acceptable inlet performance, while operating in the mode of net power extraction. We showed that the MHD region should be quite short (typically 25–30 cm along the flow) and be located as far upstream as possible. Although encouraging, those results relied upon the assumption that the magnetic coil is very large: the coil diameter was assumed to be equal to the forebody width. Minimizing the magnet size by optimizing the MHD region would be important for the practicality of the concept.

In this paper, we build upon our earlier work [2,3,10,11] and attempt to optimize the MHD region, so that the magnet size is minimized, while restoring the shock-on-lip condition and operating in the self-powered mode.

II. The Model

As in [3], we consider hypersonic gas flow along a series of compression ramps upstream of the inlet with a forward-shifted cowl lip, as schematically shown in Figs. 1 and 2. The flow is two dimensional in the (x, z) plane. Cases both without and with MHD influence on the flow are computed. In MHD cases, both magnetic field and ionizing electron beam are directed parallel to the z axis. Because the entire flow region is hypersonic, it is convenient to search for a steady-state solution using x as the marching coordinate.

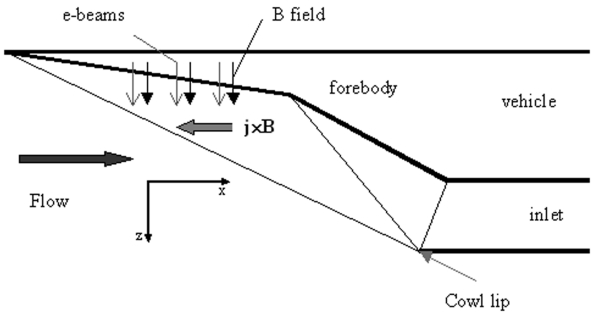

Fig. 2 Flow and shock geometry at Mach number higher than the design value, with MHD generator control.

The set of Euler equations in Cartesian coordinates, together with an ideal gas equation of state, a simple model of an ideal Faraday MHD generator, vibrational relaxation, and a plasma kinetic model, are those of [2,3]. In this paper, we only consider steady-state cases.

Two significant changes were made to the code used in [3]. First, the potentiality of the electric field, $\nabla \times \boldsymbol{E} = 0$, was enforced, which, combined with nonuniformity of flow parameters and magnetic field, results in nontrivial corrections. Indeed, consider a flow at a velocity u along the x coordinate. The magnetic field is $B = B_z$, and the electrical conductivity is σ. In general, $u = u(x, z)$, $B = B(x, z)$, and $\sigma = \sigma(x, z)$. The width of the MHD region along y will be denoted as H.

The Faraday current density is

$$j_y(x, z) = \sigma(x, z)(u(x, z)B(x, z) - E_y) \tag{1}$$

where the electric field $E_y = \text{const}$, independent of x and z, to satisfy the condition $\nabla \times \boldsymbol{E} = 0$.

The total current collected on an external resistor R_e is

$$I = \iint_{x,z} j_y(x, z)\,\mathrm{d}x\,\mathrm{d}z = \iint_{x,z} \sigma(x, z)(u(x, z)B(x, z) - E_y)\,\mathrm{d}x\,\mathrm{d}z$$
$$= \iint_{x,z} \sigma uB\,\mathrm{d}x\,\mathrm{d}z - E_y \iint_{x,z} \sigma\,\mathrm{d}x\,\mathrm{d}z \tag{2}$$

Ohm's law for the closed circuit can be written as

$$u(x, z)B(x, z)H = \frac{j_y(x, z)}{\sigma(x, z)}H + IR_e \tag{3}$$

Substituting $j_y(x, z)$ from Eq. (1) and I from Eq. (2) into Eq. (3), and solving the resulting equation for E_y, we obtain

$$E_y = \frac{R_e \iint_{x,z} \sigma uB\,\mathrm{d}x\,\mathrm{d}z}{H + R \iint_{x,z} \sigma\,\mathrm{d}x\,\mathrm{d}z} \tag{4}$$

The total electrical resistance of the nonuniform plasma region is

$$r = \frac{H}{\iint_{x,z} \sigma\,\mathrm{d}x\,\mathrm{d}z} \tag{5}$$

and the load factor is

$$k \equiv \frac{R_e}{R_e + r} = \frac{R_e}{R_e + (H/\iint_{x,z} \sigma\,\mathrm{d}x\,\mathrm{d}z)} \tag{6}$$

From Eq. (6), the external resistance R_e can be expressed in terms of the plasma conductivity and the load factor:

$$R_e = \frac{k}{1 - k}H\frac{1}{\iint_{x,z} \sigma\,\mathrm{d}x\,\mathrm{d}z} \tag{7}$$

Inserting Eq. (7) into Eq. (4), we obtain the formula for the electric field:

$$E_y = \frac{k \iint_{x,z} \sigma uB\,\mathrm{d}x\,\mathrm{d}z}{\iint_{x,z} \sigma\,\mathrm{d}x\,\mathrm{d}z} \tag{8}$$

This formula is a generalization for nonuniform cases of the familiar expression $E_y = kuB$ used in the case of uniform flow properties and magnetic fields.

MHD computations start with calculation of the electric field with formula (8). Then, local current density is found from Eq. (1). Because the conductivity and velocity profiles in the MHD region can only be determined from the computations, the computational procedure is, by necessity, iterative.

Because the field (8) is essentially an average value of uB, multiplied by k, then, according to Eq. (1), in the regions where the local uB is less than the average value times k, current will flow in the reverse direction.

External parameters of the MHD circuit, the current I and the voltage V, are calculated easily:

$$I = (1-k)\iint_{x,z} \sigma u B \,\mathrm{d}x\,\mathrm{d}z \tag{9}$$

$$V = E_y H = H\frac{k\iint_{x,z}\sigma u B\,\mathrm{d}x\,\mathrm{d}z}{\iint_{x,z}\sigma\,\mathrm{d}x\,\mathrm{d}z} \tag{10}$$

The second modification of the computational procedure relates to modeling of power deposition and ionization by the electron beams. In our earlier work [10–17], we used the so-called "forward–backward" approximation [18] for electron beam propagation along magnetic field lines into gases and beam-generated ionization. More recently, having analyzed the physics of ionization processes and the results of experiments and computations, we concluded that in a uniform gas the ionization rate profile is to be close to a truncated Gaussian [2,3]. The simplified model was then developed and used for MHD analyses [2,3]. However, the Gaussian model assumed that the electron beam is monoenergetic at its injection point. If the injected beam electrons have a range of energies, the resulting power deposition and ionization profiles can be obtained as linear superpositions of the Gaussian profiles with appropriate weights. To turn this statement around, any beam power deposition profile can be represented as a linear combination of a finite or infinite number of Gaussian profiles, corresponding to a certain initial energy spectrum of the beam electrons.

Thus, we can, in principle, select a beam power deposition profile that optimizes the MHD performance, which is done in this paper, and only then calculate the required beam energy spectrum at the injection point (this part is left for a separate future study). In fact, our preliminary analysis showed that the best performance of on-ramp MHD flow/shock control devices is reached with a near-uniform beam power deposition profile in the vertical (z) direction. Indeed, if the beam-induced ionization profile peaks close to the ramp surface, then little MHD effect exists far from the surface, resulting in little effect on the bow shock angle and cowl incidence point. If, on the other hand, ionization peaks far from the surface, the effect on the shock is substantial, but because there is little ionization in the region of the strong magnetic field (near the surface), the extracted MHD power is reduced and can be insufficient to run the ionizing electron beams. Therefore, in all calculations presented in this paper, we used a uniform profile of electron beam power deposition throughout the MHD region, characterizing the beams with power deposition density Q_b and dimensions of the ionized region along x and z.

For performance assessment of the propulsion system with and without MHD control (the detailed assessment is outside the scope of the present work), the following dimensionless parameters were computed at the inlet throat: mass capture ratio k_m; k_{p_t}; total enthalpy ratio k_H; static pressure, density, and temperature ratios k_p, k_ρ, and k_T; cooled kinetic energy efficiency $\eta_{\mathrm{KE,cool}}$; and the average Mach number M. The coefficients k for mass flow rate and static pressures, temperatures, etc., are the ratios of the respective dimensional values at the throat to the freestream values. Note that mass capture k_m is calculated by referencing the actual mass flow rate at the throat to the mass flow rate through the inlet capture area at zero angle of attack. With this definition, k_m can exceed 1.

In most cases, the flow at the inlet throat is quite nonuniform. In this work, we used the so-called stream-thrust averaging commonly accepted in inlet design [1]. This procedure, described in [1], effectively takes into account losses of total pressure (entropy increase) that would occur in the isolator when the flow is allowed to settle and to become uniform and parallel to the walls.

III. MHD Control at $M > M_{\mathrm{design}}$: Methodology of Computations, Computed Cases, and Results

The two-dimensional four-ramp inlet geometry [2], designed for Mach 5 flight at 2-deg angle of attack, is shown in Fig. 3. The ramp angles are 2.5, 8.5, 11, and 13 deg. The location of the cowl lip was chosen so that the first three oblique shocks would together reach the point slightly upstream of the lip (barely missing the lip); the fourth shock was allowed to hit the cowl. The freestream conditions at both design and off-design (Mach 8) Mach numbers studied in this paper correspond to the flight dynamic pressure of 1000 psf (47.88 kPa). Table 1 lists freestream conditions: altitude h, and static pressure and temperature, p_0 and T_0, in all computed cases.

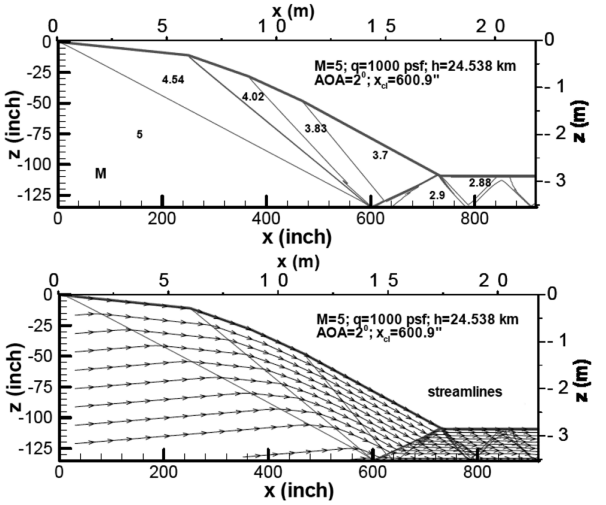

Fig. 3 Mach number contours (upper plot) and streamlines (lower plot) in the Mach 5 design case.

All computations in this work were performed with the second order MacCormack method [19] with a $12,500 \times 120$ rectangular grid, as in [3]. Information about the accuracy of the global conservation of mass, momentum, and energy is given in [3].

At Mach numbers greater than 5, the shocks would make contact with the cowl, reducing total pressure at the inlet, and potentially causing very high heat transfer rates at the shock incidence point, and possibly flow separation and engine unstart. The shock pattern and flow streamlines at off-design Mach 8 are illustrated in Fig. 4. As seen in the bottom plot of Fig. 4, the flow in the inlet is not parallel to the walls.

To maximize MHD control performance, the magnetic field should be as strong as possible, and it should protrude from the ramp into the flow as far as possible. The field was assumed to be generated by a superconducting coil placed inside the forebody and projecting magnetic field downward. The field strength at the ramp surface was assumed to be 3–5 T. The field outside the coil is a function of the ratio of the distance from the coil end plane and the coil radius. Thus, the protrusion of the B field into the gas increases with the coil diameter. Obviously, to make the magnetic field reasonably uniform in the spanwise (y) direction, noncircular magnets are needed. In the present two-dimensional modeling, however, we used the B-field strength as a circular-coil function of z, with the "effective" coil radius R that should be minimized in the modeling.

Off the centerline, the B field is not only reduced in magnitude, but it also diverges. Therefore, to maximize the ponderomotive forces pushing the flow and shocks upstream, the MHD interaction region should be concentrated near the centerline of the coil.

The ionization of air in the MHD region is created by electron beams injected from the ramp along magnetic field lines. Concentrating the electron beam current in a short region near the magnet centerline would avoid the need to have a large area of the vehicle surface covered by fragile windows or differentially pumped ports, which would have been required in cases of long, distributed

Table 1 Freestream conditions in computed cases. Freestream dynamic pressure is $q = 1000$ psf (47.88 kPa)

Mach no.	h, km	p_0, Pa	T_0, K
5	24.538	2735	221.09
8	30.76	1068.75	227.26

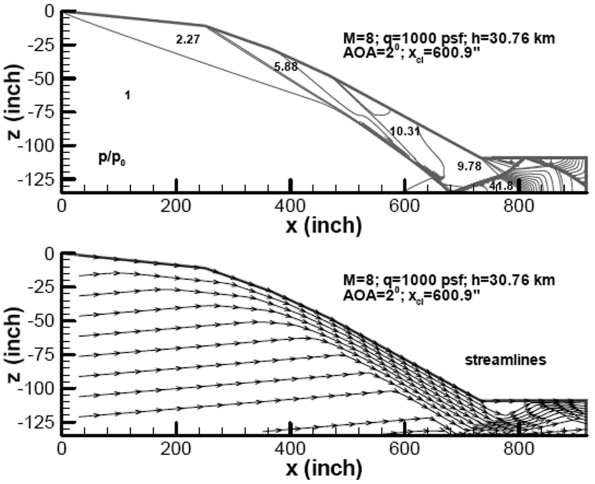

Fig. 4 Mach number contours (upper plot) and streamlines (lower plot) in the Mach 8 case without MHD control. The geometry is that of Fig. 3.

MHD interaction regions. As the MHD interaction length L becomes short, the electrical conductivity σ has to be increased to keep the interaction parameter (Stuart number) $S = \sigma B^2 L/\rho u$ (where ρ and u are the flow density and velocity), at the same level as that for a long, distributed MHD region. Because the ionization fraction and the conductivity are proportional to the square root of the electron beam current density, shortening the MHD region from 2–3 m down to 10–20 cm requires increasing the beam current density by 2 orders of magnitude, to 50–100 mA/cm^2. Aerodynamic windows or differentially pumped plasma portholes may be good candidates for electron beam transmission. Such windows or ports can presumably handle very high electron beam currents, even much higher than 100 mA/cm^2, in contrast to conventional thin foils [20].

As discussed in Sec. III, the beam power deposition profile Q_b was assumed to be uniform in the entire MHD region: $x_{\text{MHD}} \le x \le x_{\text{MHD}} + \Delta x_{\text{MHD}}$; $|z - z_b(x)| \le L_b$.

The goal of optimization studies was to find the values of parameters corresponding to restoration of the design shock wave configuration at minimal magnet radius, with MHD extracted power satisfying the constraint $P_b \approx \frac{1}{2} P_{\text{MHD}}$. The latter criterion expresses the condition that the MHD device be self-powered, that is, that the MHD generated power be just enough to generate the ionizing beams, given the approximately 50% efficiency of electron beam generation.

Table 2 MHD generator cases

Case	Q_b, MW/m^3	B_0, T	R, m	L_b, m	x_{MHD}, m	Δx_{MHD}, m	k
A_1	10	3	1.65	1.65	2	0.3	0.5
A_2	10	3	1.75	1.65	2	0.375	0.75
A_3	2	3	2	2.3	2	0.65	0.5
A_4	50	3	1.3	1	2	0.15	0.5
B	10	4	1.15	1.5	1.25	0.25	0.5
C	10	5	0.8	1.25	1	0.25	0.5
D	10	3	2.6	2.5	9	0.25	0.5
E	10	5	1.5	2.25	9	0.25	0.5

At a given MHD generator position along the forebody and B-field strength at the ramp surface, optimization parameters are the effective radius of the magnet R; e-beam penetration depth L_b; and MHD channel length Δx_{MHD}.

For the best performance, the MHD interaction region should be placed as far upstream as possible [2]. Indeed, the required linear shift of the shock incidence point at the cowl level is caused by a smaller change in the shock angle, and, therefore, by a lower MHD interaction parameter, when the MHD region is moved upstream. Additionally, creating the necessary level of ionization at lower gas density (closer to freestream conditions) requires lower current density and power of the ionizing electron beams. The two requirements for the placement of the MHD interaction region (that the interaction region should be as far upstream as possible, and that it should be close to the magnetic coil centerline) define the minimum distance of about one magnet radius of the MHD interaction region from the nose.

Thus, cases A (A_1–A_4), B, and C correspond to the MHD region placed on the first ramp, at the minimal distance from the nose. The principal parameters in these and other cases are listed in Table 2. Table 3 contains the principal MHD parameters as follows: the rate of work by $\boldsymbol{j} \times \boldsymbol{B}$ forces, $P_{j\times B}$, the extracted power P_{MHD}, the gas heating rate P_J, the power deposition into vibrational mode of molecules P_V, the power of ionizing electron beams P_b, the MHD interaction parameter S, the enthalpy extraction ratio η, the total Faraday current I_y, and the Faraday voltage U_{el}. Because of two dimensionality of the problem, all power quantities P and U_{el} are expressed per unit length (1 m) in the spanwise (y) direction. Note that the total rate of work by $\boldsymbol{j} \times \boldsymbol{B}$ forces, $P_{j\times B}$, is spent on 1) irreversible Joule heating that consists of gas heating in the narrow sense P_J, and the power deposition into vibrational mode of molecules P_V, and 2) the generated electric power P_{MHD}: $P_{j\times B} = P_{\text{MHD}} + (P_J + P_V)$. The ratio between the extracted power and the rate of dissipation is determined by the load factor. At $k = 0.5$, $P_{\text{MHD}} = P_J + P_V = 0.5 P_{j\times B}$. Note also that $P_{\text{MHD}} = I_y \times U_{\text{el}}$. The inlet performance predictions are listed in Table 4.

To demonstrate advantages of upstream placement of the MHD region, cases D and E were computed with the MHD region shifted downstream. As seen in Table 2, both R and L_b have to be increased in these cases compared with those in cases A_1 and C. Additionally, due to the more intense flow heating and the need to have a larger e-beam ionized region (longer L_b), flow spillage and reduction in air mass capture occur in cases D and E (see Table 4). Also, although cases D and E yield higher compression ratios k_p than cases A_1 and C, the better compression comes at the expense of reduced total pressure and $\eta_{\text{KE,cool}}$. Note that our numerous calculations with variation of all parameters showed that for the given design and flight conditions, it is impossible to restore the shock-on-lip condition at Mach 8 with the MHD region located at $x > 13$ m, even with a "softened" self-power condition $P_{\text{MHD}} \ge P_b$.

Cases A_1, B, and C clearly demonstrate the tradeoff between the strength of the magnetic field and the size of the magnet. Comparison of these three cases shows that the magnet size can be reduced and the shock-on-lip condition restored, if the strength of the magnetic field

Table 3 Computed MHD parameters

Case	$P_{\bar{j}\times\bar{B}}$, MW/m	P_{MHD}, MW/m	P_J, MW/m	P_V, MW/m	P_b, MW/m	S	η	I_y, kA	U_{el}, kV/m
A_1	25.4	10	9.21	6.218	4.926	0.12	0.02	6.66	1.5
A_2	22.8	11.91	7.53	3.41	6.14	0.19	0.024	5.146	2.315
A_3	32.6	11.89	1.19	8.78	2.97	0.1	0.024	8.67	1.37
A_4	7.36	7.94	6.62	3.68	7.35	0.15	0.016	4.6	1.72
B	23.33	7.82	8.33	7.17	3.72	0.19	0.016	5.23	1.49
C	20.83	6.07	7.74	7.014	3.098	0.12	0.012	4.27	1.42
D	36.71	14.88	15.03	6.8	7.47	0.1	0.03	9.52	1.56
E	46.1	14.03	18.29	13.76	6.72	0.12	0.28	9.0	1.55

Table 4 Computed inlet parameters (definitions—see Sec. III) with and without MHD control for the Mach 5 design. Angle of attack is 2^0; flight dynamic pressure is $q = 1000$ psf (47.88 kPa) for all MHD cases

Freestream Mach no. and MHD conditions	k_m	k_p	k_ρ	k_T	M	$\eta_{\mathrm{KE,cool}}$	k_H
$M = 5$; design, no MHD	1.14	16.07	6.94	2.31	2.822	0.991	1
8 No MHD	1.13	22.01	6.547	3.36	3.94	0.969	1
A_1	1.14	22.46	6.8	3.3	3.87	0.924	0.955
A_2	1.14	21.92	6.78	3.23	3.92	0.926	0.956
A_3	1.134	23.09	6.83	3.37	3.78	0.911	0.945
A_4	1.14	23.18	6.75	3.43	3.82	0.943	0.976
B	1.14	20.39	6.773	3.01	4.07	0.919	0.944
C	1.14	19.66	6.74	2.91	4.16	0.92	0.943
D	1.09	30.41	6.85	4.43	3.16	0.91	0.966
E	1.11	35.62	7.26	4.9	2.89	0.886	0.95

is increased (Table 2). However, as seen in Table 4, case A_1 is the best among these three cases in terms of compression ratio k_p, kinetic energy efficiency $\eta_{\mathrm{KE,cool}}$, and enthalpy ratio k_H. Thus, larger magnets with relatively modest B-field strength do work better than smaller magnets with stronger B.

All cases except A_2 had load factors $k = 0.5$. Case A_2 was run at a higher load factor, $k = 0.75$. As seen in Table 2, increasing the load factor requires larger magnets and longer MHD regions. Calculations at k less than 0.5, not listed in the tables, showed that the performance becomes worse than that at $k = 0.5$, because with less power extraction it is difficult to restore the design shock configuration, while demanding that $P_b \approx \frac{1}{2} P_{\mathrm{MHD}}$. Thus, for optimal performance, the load factor should not deviate far from 0.5.

Comparison of cases A_1, A_3, and A_4 demonstrates the role of the magnitude of Q_b (electron beam power deposition density). As seen in Table 2, at the given flight conditions, the value $Q_b = 10$ MW/m^3 (case A_1) is close enough to the optimum for the MHD region to be short, $\Delta x_{\mathrm{MHD}} \leq 0.3$ m, while satisfying the criterion $P_{\mathrm{MHD}} \approx \frac{1}{2} P_b$. At $Q_b = 2$ MW/m^3 (case A_3), the shock-on-lip condition can be achieved at substantially increased R, L_b, and Δx_{MHD}. At $Q_b = 50$ MW/m^3 (case A_4), the values of R, L_b, and Δx_{MHD} can be decreased as compared with those in case A_1, but only if the criterion $P_{\mathrm{MHD}} \approx \frac{1}{2} P_b$ is relaxed to $P_{\mathrm{MHD}} \approx P_b$.

Figures 5–8 show the location of the MHD region, contour lines of gas and vibrational temperature, and flow streamlines in cases A_1, C, D, and E. As seen in all those figures, due to vibrational excitation by electron impact in the MHD region and relatively slow vibrational

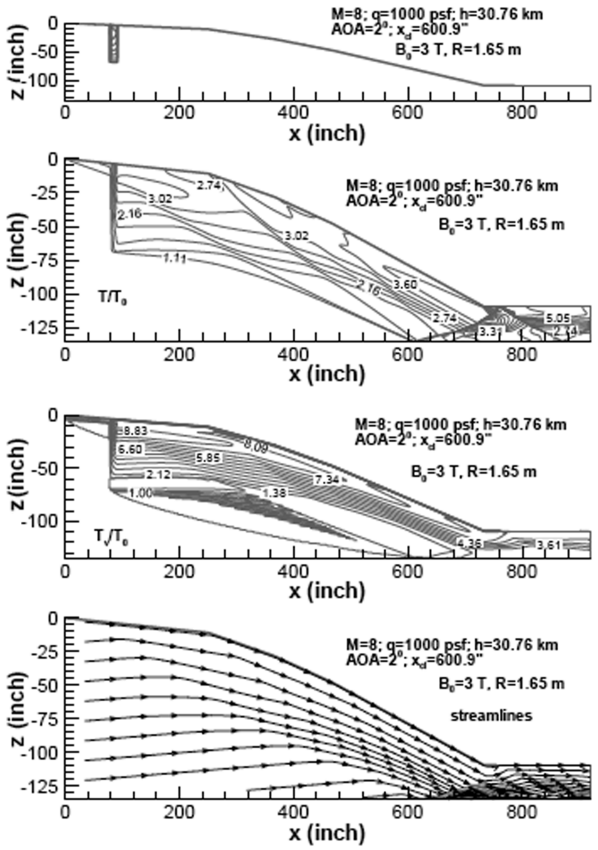

Fig. 5 Location of the MHD interaction region, contours of gas and vibrational temperatures, and streamlines at Mach 8 with MHD control for the case of a magnet with $B_0 = 3$ T; $R = 1.65$ m (case A_1).

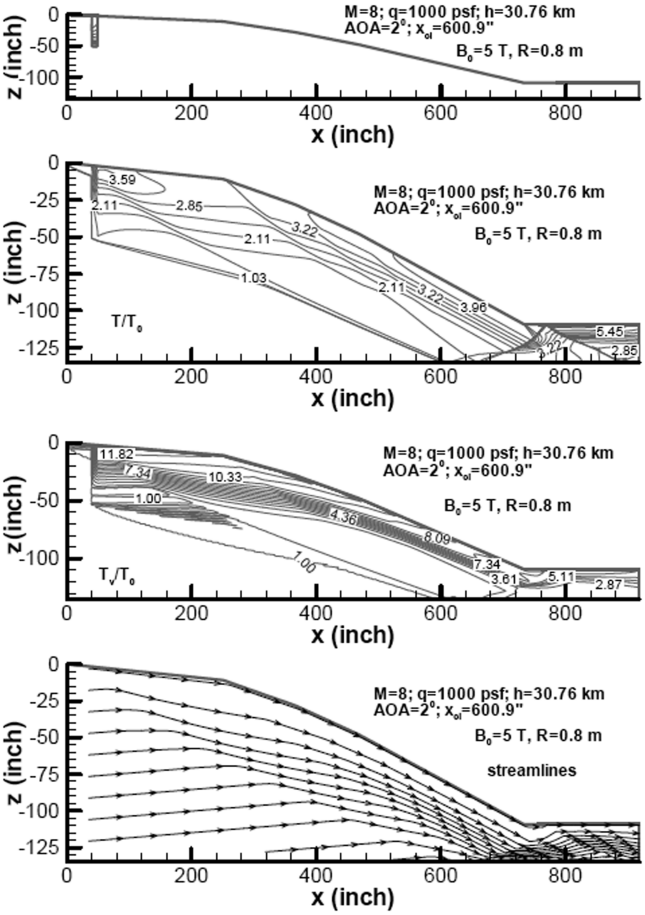

Fig. 6 Location of the MHD interaction region, contours of gas and vibrational temperatures, and streamlines at Mach 8 with MHD control for the case of a magnet with $B_0 = 5$ T; $R = 0.8$ m (case C).

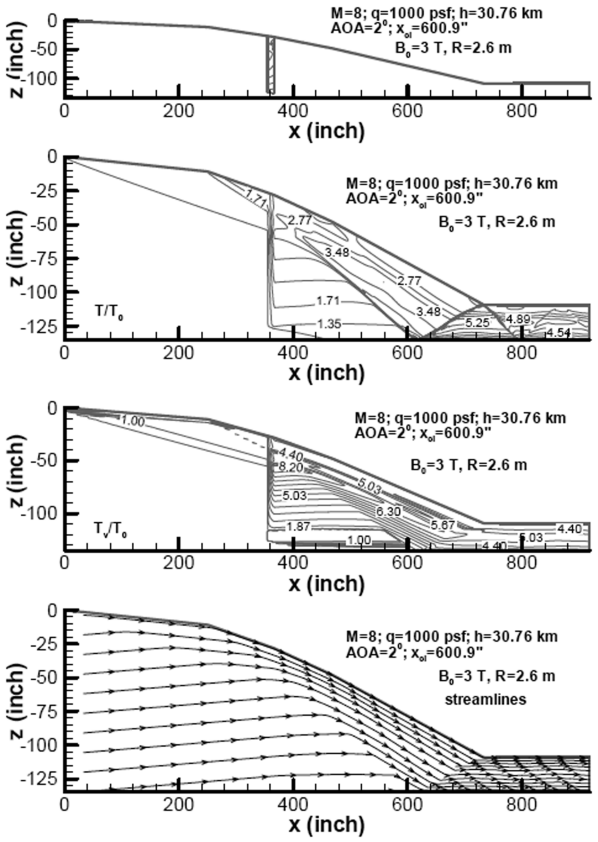

Fig. 7 Location of the MHD interaction region, contours of gas and vibrational temperatures, and streamlines at Mach 8 with MHD control for the case of a magnet with $B_0 = 3$ T; $R = 2.6$ m (case D).

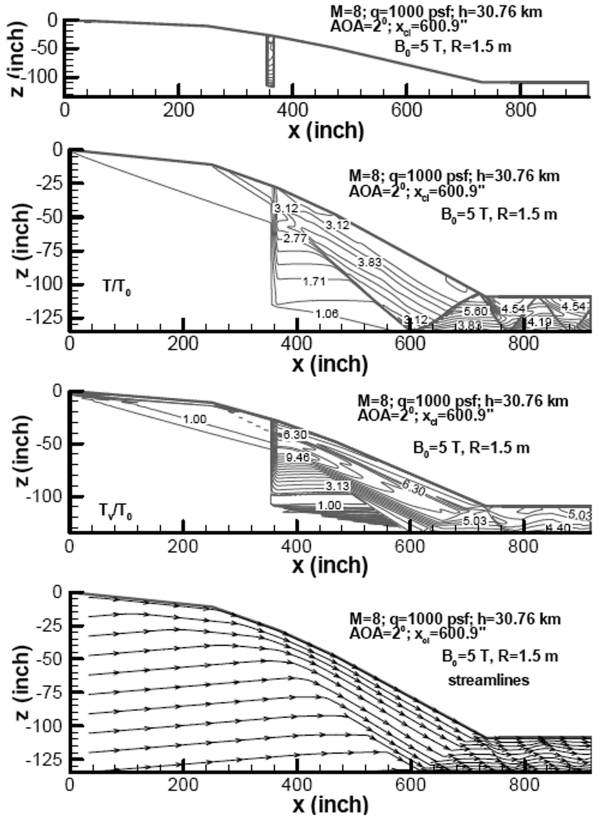

Fig. 8 Location of the MHD interaction region at Mach 8 with MHD control and contours of gas and vibrational temperatures and streamlines for the case of a magnet with $B_0 = 5$ T; $R = 1.5$ m (case E).

relaxation in the cold, low-density, weakly dissociated flow, there is a considerable vibrational nonequilibrium at the inlet throat. One challenge posed by this nonequilibrium is that the stream-thrust averaging procedure [1] was developed for thermally equilibrium flows. Fortunately, the kinetic energy efficiency $\eta_{\mathrm{KE,cool}}$ was found to be not very sensitive to the nonequilibrium conditions. Nevertheless, the procedure of stream-thrust averaging should be generalized for nonequilibrium flow in the future.

All flow calculations in this work were performed within two-dimensional inviscid approximation, as stated earlier in this paper. Viscous and three-dimensional effects can be quite important in real hypersonic flows. Therefore, the results obtained in this paper should be viewed as very approximate.

IV. Effect of Current Reversal

As discussed in Sec. II, in those areas within the MHD region where the local value of uB is less than the average value multiplied by k, the electric current should flow in the direction opposite to the Faraday electromotive force. This effect was indeed observed in all computed cases. As an example, Fig. 9 shows the current profile in case E. As seen in Fig. 9, the current density reduces to zero far from the ramp, and then becomes negative. In the region of "negative" current, the $\boldsymbol{j} \times \boldsymbol{B}$ force reverses direction and becomes an accelerating force. Although the effect was seen in all computed cases, the results were not changed much by it. However, it is conceivable that in some other MHD problems the current reversal can play a significant role.

Consider, for example, the near-wall region of an MHD generator. If the B field is normal to the surface, and the conductivity is more or less uniform across the boundary layer, then close enough to the wall, where the velocity is less than the freestream velocity multiplied by the load factor, the $\boldsymbol{j} \times \boldsymbol{B}$ will accelerate the boundary layer. This effect can, in principle, change the boundary layer structure and thickness, and can affect vorticity generation, flow separation, and laminar-turbulent transition. These phenomena should be investigated in the future.

V. Conclusions

The principal conclusion that can be drawn from the modeling described in this paper is that, with a proper choice of parameters, a short (25–30 cm) MHD generator placed at the first compression ramp can restore the design (Mach 5) shock configuration in the Mach 8 flight, while operating in self-powered mode, with the MHD generated power sufficient for generation of the ionizing electron beams. The modeling shows that there is a tradeoff between reducing the magnet size and increasing the strength of the magnetic field, and that the magnet size can be substantially reduced compared with our earlier nonoptimized studies.

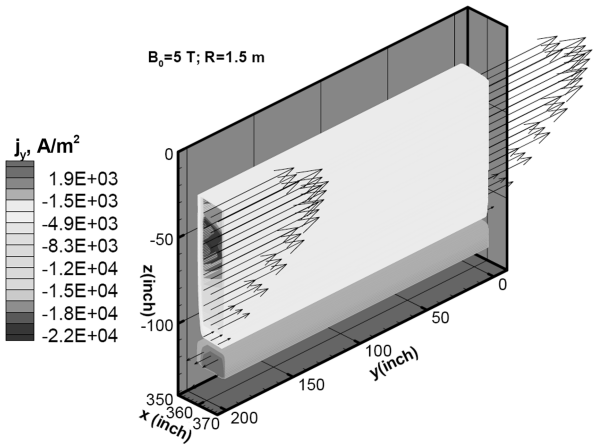

Fig. 9 Current density profile and directions in the MHD region for the case of Fig. 8 (case E).

The predicted effect of electric current reversal and local MHD acceleration in nonuniform MHD generators, although quantitatively not strong in the computed cases, can nevertheless be of importance in other MHD problems, possibly including boundary layers, flow separation, and turbulence control.

Acknowledgments

This work was supported by Boeing Phantom Works, Defense Advanced Research Projects Agency (DARPA), Johns Hopkins University Applied Physics Laboratory, and by the U.S. Air Force Office of Scientific Research. The authors express their gratitude to Joseph Silkey and Philip Smereczniak of Boeing Phantom Works, to David Van Wie of Johns Hopkins University Applied Physics Laboratory, and to Ramon Chase of ANSER Corporation for guidance, valuable discussions, and advice.

References

[1] Van Wie, D. M., "Scramjet Inlets," *Scramjet Propulsion*, edited by E. T. Curran, and S. N. B. Murthy, Vol. 189, Progress in Astronautics and Aeronautics, AIAA, Reston, VA, 2000, pp. 447–511, Chap. 7.

[2] Shneider, M. N., Macheret, S. O., and Miles, R. B., "Nonequilibrium Magnetohydrodynamic Control of Scramjet Inlets," AIAA Paper 2002-2251, 20–23 May 2002.

[3] Shneider, M. N., Macheret, S. O., and Miles, R. B., "Analysis of Magnetohydrodynamic Control of Scramjet Inlets," *AIAA Journal*, Vol. 42, No. 11, Nov. 2004, pp. 2303–1210.

[4] Kuranov, A. L., and Sheikin, E. G., "MHD Control on Hypersonic Aircraft Under AJAX Concept: Possibilities of MHD Generator," AIAA Paper 2002-0490, 2002.

[5] Vatazhin, A., Kopchenov, V., and Gouskov, O., "Some Estimations of Possibility to Use the MHD Control for Hypersonic Flow Deceleration," AIAA Paper 99-4972, 1999.

[6] Kopchenov, V., Vatazhin, A., and Gouskov, O., "Estimation of Possibility of Use of MHD Control in Scramjet," AIAA Paper 99-4971, 1999.

[7] Vatazhin, A., Kopchenov, V., and Gouskov, O., "Numerical Investigation of Hypersonic Inlets Control by Magnetic Field," *The 2nd Workshop on Magneto- and Plasma Aerodynamics in Aerospace Applications*, Russian Academy of Sciences, Institute of High Temperatures (IVTAN), Moscow, 5–7 April 2000, pp. 56–63.

[8] Brichkin, D. I., Kuranov, A. L., and Sheikin, E. G., "The Potentialities of MHD Control for Improving Scramjet Performance," AIAA Paper 99-4969, 1999.

[9] Bityurin, V. A., Klimov, A. I., Leonov, S. B., Bocharov, A. N., and Lineberry, J. T., "Assessment of a Concept of Advanced Flow/Flight Control for Hypersonic Flights in Atmosphere," AIAA Paper 99-4820, 1999.

[10] Macheret, S. O., Shneider, M. N., and Miles, R. B., "External Supersonic Flow and Scramjet Inlet Control by MHD with Electron Beam Ionization," AIAA Paper 2001-0492, 2001.

[11] Macheret, S. O., Shneider, M. N., and Miles, R. B., "Magnetohydrodynamic Control of Hypersonic Flow and Scramjet Inlets Using Electron Beam Ionization," *AIAA Journal*, Vol. 40, No. 1, 2002, pp. 74–81.

[12] Macheret, S. O., Shneider, M. N., and Miles, R. B., "Magnetohydrodynamic and Electrohydrodynamic Control of Hypersonic Flows of Weakly Ionized Plasmas," AIAA Paper 2002-2249, 20–23 May 2002.

[13] Macheret, S. O., Shneider, M. N., Miles, R. B., Lipinski, R. J., and Nelson, G. L., "MHD Acceleration of Supersonic Air Flows Using Electron Beam-Enhanced Conductivity," AIAA Paper 98-2922, 1998.

[14] Macheret, S. O., Shneider, M. N., and Miles, R. B., "Electron Beam Generated Plasmas in Hypersonic MHD Channels," AIAA Paper 99-3635, 1999.

[15] Macheret, S. O., Shneider, M. N., and Miles, R. B., "MHD Power Extraction from Cold Hypersonic Air Flow with External Ionizers," AIAA Paper 99-4800, 1999.

[16] Macheret, S. O., Shneider, M. N., and Miles, R. B., "MHD Power Extraction from Cold Hypersonic Air Flow with External Ionizers," *Journal of Propulsion and Power*, Vol. 18, No. 2, 2002, pp. 424–431.

[17] Macheret, S. O., Shneider, M. N., Miles, R. B., and Lipinski, R. J., "Electron Beam Generated Plasmas in Hypersonic Magnetohydrodynamic Channels," *AIAA Journal*, Vol. 39, No. 6, 2001, pp. 1127–1136.

[18] Raizer, Y. P., and Shneider, M. N., "Simplified Kinetic Equation for Electrons in Nonuniform Fields of Arbitrary Strength in Connection with the Cathode Sheath of a Glow Discharge," *Soviet Journal of Plasma Physics*, Vol. 15, No. 3, 1989, pp. 184–189.

[19] Anderson, D. A., Tannehill, J. C., and Pletcher, R. H., *Computational Fluid Mechanics and Heat Transfer*, Hemisphere, New York, 1984.

[20] Hershcovitch, A., "A Plasma Window for Transmission of Particle Beams and Radiation From Vacuum to Atmosphere for Various Applications," *Physics of Plasmas*, Vol. 5, No. 5, 1998, pp. 2130–2136.

G. Candler
Associate Editor